analytical chemistry

pubs.acs.org/ac Article

Modulating Polarization of Perovskite-Based Heterostructures via In Situ Semiconductor Generation and Enzyme Catalysis for Signal-Switchable Photoelectrochemical Biosensing

Hao Yang, Min Zhang, Lei Wang, Renzhong Yu, Wenwen Tu, Zhaoyin Wang,* Rui Wang, Huan Gao, and Zhihui Dai*

Cite This: *Anal. Chem.* 2021, 93, 8370−8378 Read Online

ACCESS | Metrics & More | Article Recommendations | Supporting Information

ABSTRACT: Polarization of photoactive materials in current photoelectric (PE) systems is difficult to be adjusted, and thus electron-transfer routes of these systems are unchangeable, which limits their performance in photoelectrochemical (PEC) analysis. Herein, we attempted to modulate the polarization of perovskite-based heterostructures by both in situ semiconductor generation and enzyme catalysis. Owing to their band alignments, $Cs_3Bi_2Br_9$ quantum dots (QDs) and BiOBr are confirmed to construct a Z-scheme structure, leading to a large anodic photocurrent. In the presence of ascorbic acid 2-phosphate (AAP), $BiPO_4$ is generated on the surface of the $Cs_3Bi_2Br_9$ QDs/BiOBr heterostructure, reassigning energy bands of BiOBr. Accordingly, polarization of the photoactive materials is converted, and a new Z-scheme structure with a reversed electron-transfer route is constructed, which leads to an evident cathodic photocurrent. Furthermore, abundant electron donors can be obtained by catalyzing AAP with alkaline phosphatase (ALP). In this case, photogenerated holes in BiOBr are preferentially annihilated by electron donors, thereby blocking transfer of photogenerated electrons in the $Cs_3Bi_2Br_9$ QDs/BiOBr/$BiPO_4$ heterostructure. Consequently, a second polarization conversion is triggered by enzyme catalysis, resulting in the recovery of an anodic photocurrent. Benefited from the polarization conversion, a PEC biosensor with a feature of two-wing signal switch is designed, which remarkably enlarges the range of the signal response and subsequently improves the analytical performance. As a result, ALP in small volume of human serum can be quantified with this method. In this work, polarization of perovskite-based photoactive materials is tuned, proposing an alternative perspective on the design of advanced PE systems.

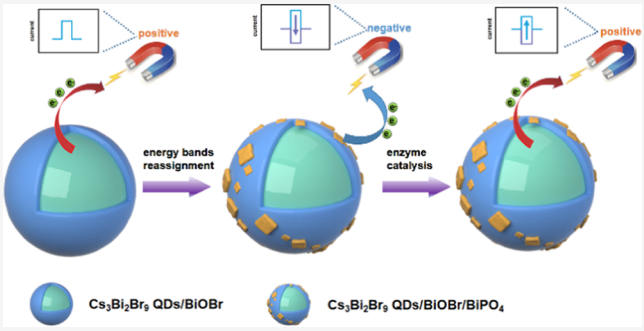

INTRODUCTION

Due to their prominent feature of adjustable polarization,[1−3] photoelectric (PE) systems are able to exhibit a PE response in two wings, i.e., anodic and cathodic responses. Manipulation of polarization may adjust electron-transfer routes, enabling switch of the PE response from one wing to the other, which improves performance of PE systems including photoelectrochemical (PEC) sensors. It is well known that photoactive materials reveal a certain PE response in the presence of a suitable bias and a matched electron donor or acceptor.[4,5] In other words, the electron-transfer route of a PE process is determined by a photoactive material, bias, and redox conditions (species and number of electron donor and acceptor). In comparison with bias regulation, tuning of photoactive materials and redox conditions is effective but difficult to attain because the two factors are normally restrictive for PE systems. Therefore, controllable polarization modulation to achieve a PE response switch from one wing to the other is still challenging but urgently needed to develop high-performance PE systems.

To date, most of PEC-based analytical approaches are established on the basis of the one-wing response switch,[6−8] and thus inherent superiority of PE systems has not been thoroughly embodied in current PEC sensors. To our knowledge, the few studies related to PEC conversion are realized by tuning electron-transfer efficiency rather than electron-transfer routes,[9−11] thereby not relevant to polarization modulation. In these PEC systems, more than one photoactive material generates anodic and cathodic PEC responses individually. With the change in anodic and cathodic PEC responses in different cases, the overall signals may be altered from anodic or cathodic responses to the opposite

Received: April 6, 2021
Accepted: May 18, 2021
Published: May 27, 2021

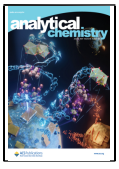

https://doi.org/10.1021/acs.analchem.1c01457
Anal. Chem. 2021, 93, 8370−8378

Scheme 1. Schematic Illustration of a PEC Sensing Platform for the Detection of ALP in a Two-Wing Signal Switch Manner

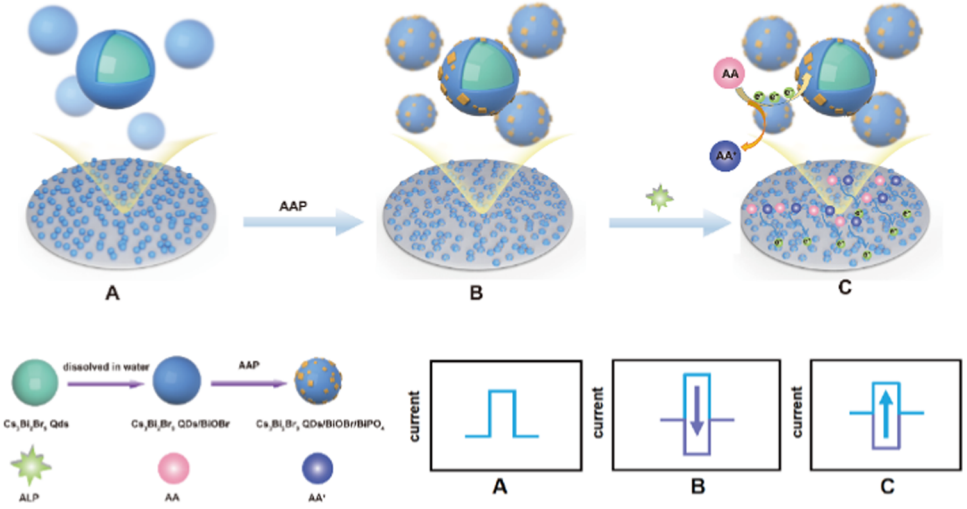

ones, while polarization of these PEC systems is not essentially adjusted. To achieve "real" polarization conversion, more efforts should be devoted to tuning properties of photoactive materials and adjusting redox conditions. Compared with hybridization of diverse materials, in situ generation of new semiconductors on the surface of other materials is conductive to forming compound materials with heterostructures,[12,13] which is helpful to fulfill polarization modulation. On one hand, formation of heterostructures may regulate the energy bands of compound materials[14−16] and allow a band match between new semiconductors and original materials, directly modulating the polarization of photoactive materials. On the other hand, in situ generation of semiconductors ensures physical contact of different photoactive materials, facilitating the electron transfer and enhancing the effect of heterostructures on polarization modulation. In addition, enzyme catalysis is capable of effectively changing species and number of redox molecules, such as electron donors and acceptors.[17−19] Under the catalysis of enzymes, redox conditions of PEC systems may be changed, subsequently altering the polarization, which eventually results in the switch of PEC responses. Based on the aforementioned reason, in situ generation of photoactive materials and enzyme catalysis-enabled regulation of redox molecules are promising strategies to achieve polarization modulation, which is of high value in establishing PEC systems with the feature of two-wing response switch.

Besides long diffusion length, low cost in synthesis, and composition diversity,[20−22] perovskites have been considered to be one of the outstanding photoactive materials for their long carrier lifetime, large light absorption coefficient, and high photo-to-electric conversion efficiency.[23−26] However, perovskite-based PEC sensors have rarely been reported because pure perovskites, Pb-contained perovskites, in particular, are normally toxic and unstable in water.[27,28] In comparison with other photoactive materials, perovskites possess abundant IVA and VA elements,[29] which are suitable to in situ semiconductor formation on the outside of perovskites. With the protection of the outer semiconductor layer, toxicity of inner perovskites is remarkably reduced, while stability in water is significantly improved. More importantly, formation of perovskite/semiconductor heterostructures may reassign band gaps of perovskites and semiconductors,[30,31] modulating the polarization of the whole PEC systems, which makes the adjustment of electron-transfer routes possible.

Herein, polarization of a perovskite/semiconductor heterostructure is modulated by in situ generation of a semiconductor layer and enzyme catalysis-induced electron donor production, which is further employed to establish a PEC biosensor with enhanced analytical performance. Because a Z-scheme structure is established with $Cs_3Bi_2Br_9$ quantum dots (QDs) and BiOBr,[32] the $Cs_3Bi_2Br_9$ QDs/BiOBr heterostructure exhibits a large anodic photocurrent. To tune the electron-transfer route, we attempted to further introduce a second semiconductor that matches the energy bands of BiOBr. By employing ascorbic acid 2-phosphate (AAP), $BiPO_4$ can be generated on the surface of the $Cs_3Bi_2Br_9$ QDs/BiOBr heterostructure, reassigning energy bands of BiOBr and constructing a new Z-scheme. As a result, the electron-transfer route in the $Cs_3Bi_2Br_9$ QDs/BiOBr/$BiPO_4$ heterostructure is reversed, leading to the PEC signal switch from anodic photocurrents to cathodic photocurrents. AAP can be hydrolyzed to produce ascorbic acid (AA) by alkaline phosphatase (ALP).[33] With the emergence of plenty of AA, the electron transfer from BiOBr to $BiPO_4$ is impeded. Accordingly, polarization of the $Cs_3Bi_2Br_9$ QDs/BiOBr/$BiPO_4$ heterostructure is converted for a second time, and cathodic photocurrents become anodic ones again. Relying on the polarization modulation caused by the in situ semiconductor generation and enzyme catalysis, ALP is sensitively quantified in a two-wing signal switch manner (Scheme 1).

EXPERIMENTAL SECTION

Reagents and Materials. Tris (hydroxymethyl) aminomethane (Tris) was purchased from Alfa Aesar. Cesium bromide (CsBr), octylamine (OLAm), and oleic acid (OA) were purchased by Aladdin Industrial Corporation. Bismuth tribromide ($BiBr_3$) was purchased by Shanghai Macklin Biochemical Co., Ltd. Potassium bromide (KBr), sodium hydroxide (NaOH), dimethyl sulfoxide (DMSO), bismuth nitrate ($Bi(NO_3)_3$), calcium chloride ($CaCl_2$), magnesium chloride ($MgCl_2$), potassium chloride (KCl), ethanol, and ethylene glycol were provided by Sinopharm Chemical Reagent Co., Ltd. (China). Acid 2-phosphate sesquimagnesium salt (AAP) was purchased by Shanghai Yuanye Bio-Technology Co., Ltd. Tyrosine (Tyr), threonine (Thr), uric

https://doi.org/10.1021/acs.analchem.1c01457
Anal. Chem. 2021, 93, 8370−8378

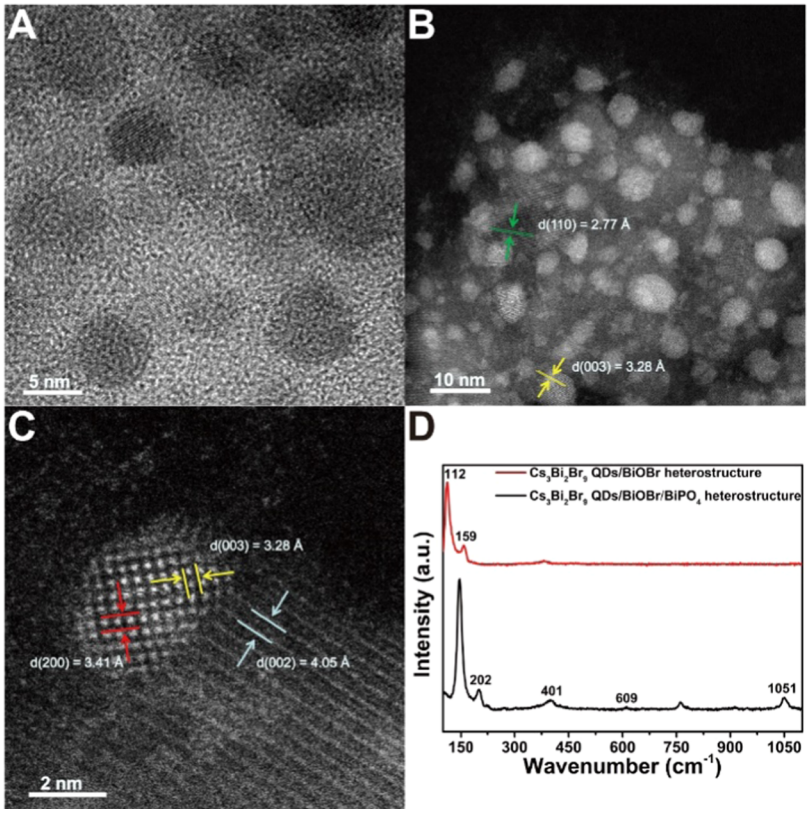

Figure 1. (A) HRTEM image of $Cs_3Bi_2Br_9$ QDs. (B) and (C) HAADF-STEM images of the $Cs_3Bi_2Br_9$ QDs/BiOBr heterostructure. (D) Raman spectra of the $Cs_3Bi_2Br_9$ QDs/BiOBr and $Cs_3Bi_2Br_9$ QDs/BiOBr/$BiPO_4$ heterostructures.

acid (UA), glucose (Glu), pyrophosphatase (PPase), alkaline phosphatase (ALP), and 3-(4,5-dimethyl-2-thiazolyl)-2,5-diphenyl-2*H*-tetrazolium bromide (MTT) were all purchased from Shanghai Sangon Biological Engineering Technology and Services Co., Ltd. (China). Glucose oxidase (GOx) and horseradish peroxidase (HRP) were obtained from Sigma-Aldrich Co., Ltd. (China). 1-Ethyl-3-methylimidazolium tetrafluoroborate (ion liquid) was purchased by Shanghai Chengjie Chemical Co., Ltd. The working electrode indium tin oxide (ITO) slices (20−25 Ω/sq) were acquired from Jintan Kondrk Photoelectric Science & Technology Co., Ltd. (China). Solutions were prepared using ultrapure water (18.2 MΩ cm) provided by a Milli-Q purification system (Bedford, MA). Human serum samples were obtained from Jiangsu Provincial Cancer Hospital and used with the approval of the Ethical Committee of Nanjing Normal University (No. IACUC-20200601).

Apparatus. Transmission electron microscopy (TEM) images were taken using a Hitachi H-7650 type transmission electron microscope with an accelerating voltage of 80 kV (Hitachi, Japan). High-resolution transmission electron microscopy (HRTEM) images were obtained using a JEOL-2100F apparatus at an accelerating voltage of 200 kV. Atomic structures (high-angle annular dark-field scanning transmission electron microscopy, HAADF-STEM images) of the $Cs_3Bi_2Br_9$ QDs/BiOBr were taken using an ARM-200CF transmission electron microscope operated at 200 kV, equipped with double spherical aberration (Cs) correctors. The X-ray powder diffraction (XRD) pattern was obtained using a D/max 2500 VL/PC diffractometer (Japan) equipped with graphite monochromatized Cu Kα radiation. PEC measurements and Mott−Schottky measurements were performed on a Zahner PEC workstation (Zahner, Germany). All experimental tests were performed by a conventional three-electrode system at room temperature. A modified ITO electrode with a geometric area of 0.28 cm^2 was acting as a working electrode, a platinum wire was acting as an auxiliary electrode, and a Ag/AgCl electrode was applied as a reference electrode. Raman spectra were tested by a microconfocal spectrometer-HR Evolution with a 633 nm laser at a power of 100 mW. Electron spin resonance (ESR) signals were recorded on a Bruker A300 (X-band) spectrometer (Bruker, Germany). UV−vis diffuse reflectance spectra (DRS) were obtained using a Cary 5000 UV−Vis−NIR Spectrophotometer (Varian). MTT assays were measured at 490 nm using a microplate reader (Thermo Scientific Multiskan GO).

Synthesis of $Cs_3Bi_2Br_9$ QDs. $Cs_3Bi_2Br_9$ QDs were synthesized by a traditional one step-method.[32] First, 42.562 mg of CsBr and 60.125 mg of $BiBr_3$ as well as 33 μL of OLAm were dissolved into 3 mL of DMSO to form a $Cs_3Bi_2Br_9$ precursor solution. Then, 0.5 mL of OA was dissolved into 5 mL of ethanol. Afterward, the solution was slowly dropped into a three-neck flask and stirred vigorously at 80 °C. Subsequently, 0.5 mL of the precursor solution was slowly dropped into the mixture of 0.5 mL of OA and 5 mL of ethanol for 10 min. After that, the mixed solution was taken out and cooled to room temperature. After the solution cooled down to room temperature, gradient centrifugation was used at 5000 rpm and then 10 000 rpm both for 10 min. Afterward, the precipitation of $Cs_3Bi_2Br_9$ QDs was obtained and then dried in an oven for 24 h to get the $Cs_3Bi_2Br_9$ QD powders. The solid powders were collected for later use.

Preparation of BiOBr. BiOBr was produced by dissolving 0.01 mol KBr into 50 mL of ethylene glycol solution; then, the

https://doi.org/10.1021/acs.analchem.1c01457
Anal. Chem. 2021, 93, 8370−8378

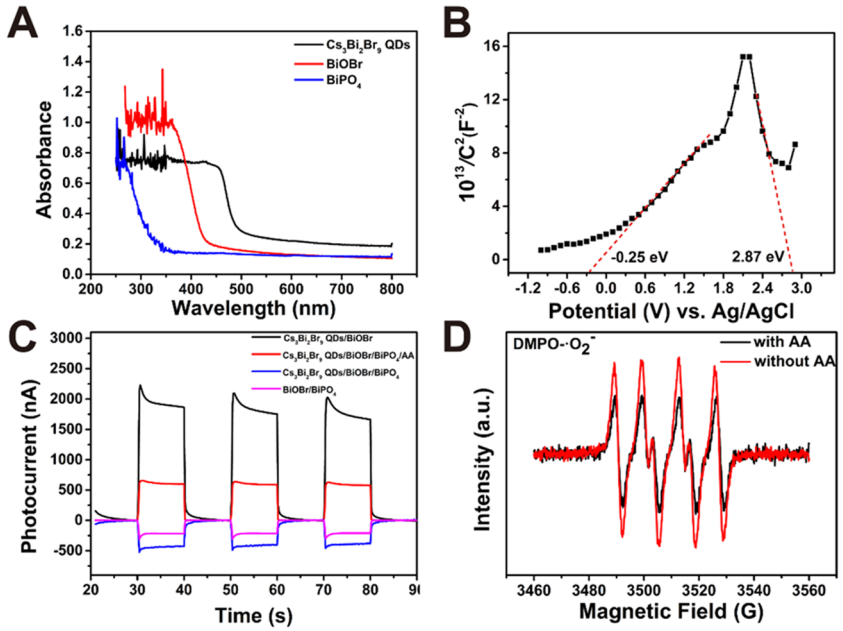

Figure 2. (A) Solid UV−vis diffuse reflectance spectra of $Cs_3Bi_2Br_9$ QDs, BiOBr, and $BiPO_4$. (B) Mott−Schottky curve of the $Cs_3Bi_2Br_9$ QDs/BiOBr heterostructure. (C) Photocurrent responses of the $Cs_3Bi_2Br_9$ QDs/BiOBr heterostructure, the $Cs_3Bi_2Br_9$ QDs/BiOBr/$BiPO_4$ heterostructure, the BiOBr/$BiPO_4$ heterostructure, and the $Cs_3Bi_2Br_9$ QDs/BiOBr/$BiPO_4$ heterostructure in the presence of AA. (D) ESR curves of the $Cs_3Bi_2Br_9$ QDs/BiOBr/$BiPO_4$ heterostructure in the absence or presence of AA.

solution was added dropwise into 50 mL of $Bi(NO_3)_3$ in ethylene glycol (0.2 mol/L). The mixture was stirred for 30 min at room temperature and then transferred into a Teflon autoclave. After that, the autoclave was heated at 160 °C for 12 h and cooled down to room temperature. The final product was separated by centrifugation, washed with distilled water and ethanol, and dried under vacuum at 80 °C for 24 h before further characterizations.

Construction of the $Cs_3Bi_2Br_9$ QD-Modified Electrode. ITO electrodes were put in a beaker filled with acetone and treated by ultrasonication for 15 min. Then, the electrodes were washed with deionized water. After that, the electrodes were washed with 1 M NaOH/ethanol mixed solution (v/v, 1:1) and deionized water both for 15 min. Finally, the ITO electrodes were dried in an oven at 60 °C for 2 h. To prepare a $Cs_3Bi_2Br_9$ QD-modified electrode, 2 mg of $Cs_3Bi_2Br_9$ QDs was dissolved in 1 mL of water, and 20 μL of the $Cs_3Bi_2Br_9$ QD solution was dropped on the ITO electrode surface. After drying for 30 min in the oven at 37 °C, the electrode was ready for later use.

Detection of ALP. Different concentrations of ALP and 44 μM of AAP were mixed with the same volume and incubated in an oven at 37 °C for 25 min. After the incubation, 20 μL of the mixture was dropped on the surface of the $Cs_3Bi_2Br_9$ QDs and dried at 37 °C in the oven for 30 min. Finally, the obtained electrode was ready for PEC measurements. Under 365 nm light irradiation, PEC measurements were carried out in Tris-HCl buffer saline (0.1 M, pH 7.4) with the applied potential of 0.15 V.

RESULTS AND DISCUSSION

Characterization of Photoactive Materials with Different In Situ Generated Semiconductors. All inorganic perovskite $Cs_3Bi_2Br_9$ QDs are chosen as basal photoactive materials since the Pb-free perovskite QDs have low toxicity and possess larger specific surface areas for in situ generation of an outer layer. It has been reported that $Cs_3Bi_2Br_9$ QDs are passivated in water by forming a BiOBr layer.[32] Morphological properties of the $Cs_3Bi_2Br_9$ QDs/BiOBr heterostructure were first studied. As shown in Figures 1A, S1, and S2, the monodisperse $Cs_3Bi_2Br_9$ QDs are quasi-spherical with a diameter of 4.8 ± 0.9 nm, indicating that the perovskite may possess a strong quantum confinement effect. For the sample of $Cs_3Bi_2Br_9$ QDs dissolved in water, the morphology of the nanomaterials is remarkably changed. Typical lattice spacings representing BiOBr and $Cs_3Bi_2Br_9$ can be evidently observed in high-angle annular dark-field scanning transmission electron microscopy (HAADF-STEM) images (Figure 1B,C), certifying the generation of a BiOBr layer on the base of $Cs_3Bi_2Br_9$ QDs. To be specific, the interplanar distances of 3.28 and 3.41 Å correspond to the (003) and (200) crystal planes of $Cs_3Bi_2Br_9$, while those of 2.77 and 4.05 Å are assigned to the (110) and (002) crystal planes of BiOBr. By treating the $Cs_3Bi_2Br_9$ QDs/BiOBr heterostructure with AAP, typical bands representing O−Bi−O and PO_4^{3-} can be recorded in the Raman spectrum (Figure 1D). As for the pure $Cs_3Bi_2Br_9$ QDs/BiOBr heterostructure, the band centered at 112 cm^{-1} belongs to the A_{1g} internal Bi−Br stretching modes, while that centered at 159 cm^{-1} should be assigned to the E_{1g} internal Bi−Br stretching modes. If the $Cs_3Bi_2Br_9$ QDs/BiOBr heterostructure is treated with AAP, additional bands can be recorded in the Raman spectrum. The band at 202 cm^{-1} is due to a symmetric bending mode of O−Bi−O.[34] In addition, bending modes of PO_4^{3-} are reflected by the bands at 401 and 609 cm^{-1}, and the intense band at 1051 cm^{-1} represents an antisymmetric ν_3 stretching mode of PO_4^{3-}.[35,36] These results demonstrate that $BiPO_4$ can be in situ synthesized on the surface of the $Cs_3Bi_2Br_9$ QDs/BiOBr heterostructure, forming a new kind of perovskite/semiconductor complex.

Polarization Conversion of Perovskite-Based Heterostructures by In Situ Generation of $BiPO_4$ and ALP-Induced Catalysis. Having confirmed the formation of

https://doi.org/10.1021/acs.analchem.1c01457
Anal. Chem. 2021, 93, 8370−8378

Scheme 2. Possible Mechanism of Polarization Conversion Induced by In Situ Semiconductor Generation and Enzyme Catalysis

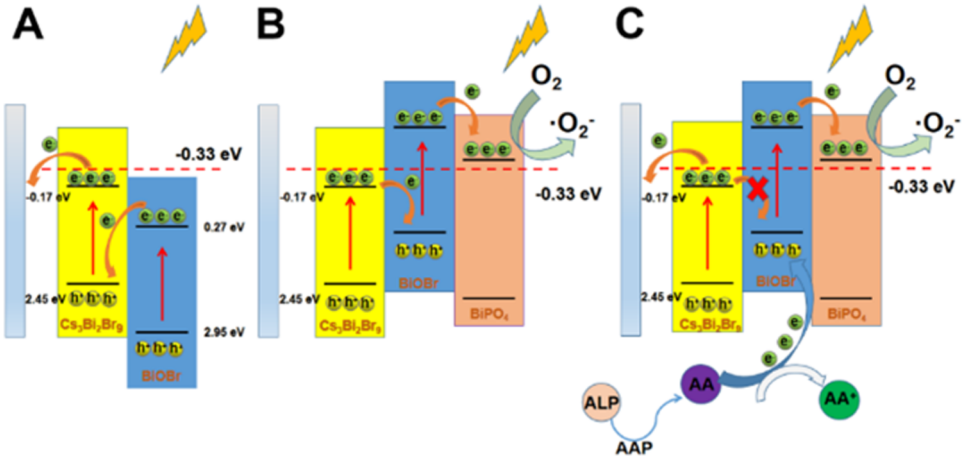

$Cs_3Bi_2Br_9$ QDs, the $Cs_3Bi_2Br_9$ QDs/BiOBr heterostructure, and the $Cs_3Bi_2Br_9$ QDs/BiOBr/$BiPO_4$ heterostructure, we further investigated the PEC behavior of these photoactive materials. According to the Mott−Schottky curves (Figures S3A, S4A, S5A, and S5B), $Cs_3Bi_2Br_9$ QDs are n-type semiconductors with an anodic photocurrent of 178 nA, while BiOBr is a p-type semiconductor with a cathodic photocurrent of −20 nA. Meanwhile, the flat band potentials of the two semiconductors are −0.07 and 2.95 eV versus normal hydrogen electrode (NHE). Furthermore, the band gaps of $Cs_3Bi_2Br_9$ QDs and BiOBr were identified to be 2.62 and 2.68 eV by analyzing solid ultraviolet−visible (UV−vis) diffuse reflectance spectra with the Kubelka−Munk (KM) method (Figures 2A, S3B, and S4B). In comparison with single $Cs_3Bi_2Br_9$ QDs or BiOBr, the $Cs_3Bi_2Br_9$ QDs/BiOBr heterostructure exhibits two slopes in the Mott−Schottky curve but possesses similar flat band potentials (Figure 2B). The results indicate that $Cs_3Bi_2Br_9$ QDs and BiOBr only physically contact in the $Cs_3Bi_2Br_9$ QDs/BiOBr heterostructure, which will not alter their energy band alignment. Since the conduction band potential (E_{CB}) of BiOBr is in the middle of the E_{CB} and the valence band potential (E_{VB}) of $Cs_3Bi_2Br_9$ QDs, photogenerated electrons can transfer in the $Cs_3Bi_2Br_9$ QDs/BiOBr heterostructure in a "Z-scheme" manner, which can be confirmed by the enhancement of the photocurrent response (Figure S5C). Formation of the Z-scheme structure facilitates separation of photogenerated electrons and holes and subsequently leads to a large anodic photocurrent of 1952 nA (Figure 2C). However, the $Cs_3Bi_2Br_9$ QDs/BiOBr/$BiPO_4$ heterostructure reveals an unexpected PE response switch from anodic photocurrents to cathodic ones (Figure S6), suggesting that the polarization conversion occurs due to the generation of $BiPO_4$. Since $BiPO_4$ is generated with the participation of AAP, the PEC response of pure AAP was tested and determined to be negligible (Figure S5D). Results of electron spin resonance (ESR) reveal that the $Cs_3Bi_2Br_9$ QDs/BiOBr/$BiPO_4$ heterostructure is capable of producing $^{\bullet}O_2^-$ under the excitation of light (Figures 2D and S7), indicating that photogenerated electrons are transferred to a potential more negative than E(O_2/$^{\bullet}O_2^-$) (−0.33 eV versus NHE).[37] Based on the data of the solid UV−vis diffuse reflectance spectrum and the Mott−Schottky curve (Figures 2A and S8), $BiPO_4$ is confirmed to be an n-type semiconductor with E_{VB} and E_{CB} of 3.54 and −0.66 eV versus NHE, respectively. With such a big band gap, $BiPO_4$ cannot be excited under the illustration of 365 nm light. Measured data indicate that E_{CB} of $Cs_3Bi_2Br_9$ QDs is −0.17 eV versus NHE and is incompetent to reduce oxygen to generate $^{\bullet}O_2^-$. In addition, previous studies demonstrate that the energy bands of BiOBr are higher than those of $BiPO_4$ in the BiOBr/$BiPO_4$ heterostructure.[38,39] Therefore, it can be concluded that generation of $BiPO_4$ reassigns energy bands of the $Cs_3Bi_2Br_9$ QDs/BiOBr heterostructure, increasing the E_{CB} of BiOBr more negative than −0.33 eV. To be noted, the photocurrent of the $Cs_3Bi_2Br_9$ QDs/BiOBr/$BiPO_4$ heterostructure is larger than that of the BiOBr/$BiPO_4$ heterostructure, indicating that some electrons are transferred from CB of $Cs_3Bi_2Br_9$ QDs to VB of BiOBr. Accordingly, the original Z-scheme is replaced with a new Z-scheme, which leads to a large cathodic photocurrent. By treating AAP with ALP, a second polarization conversion is observed. The produced AA, a well-known electron donor, is prone to inject electrons into photogenerated holes with the most negative potential. As a result, photogenerated holes in VB of BiOBr are filled with electrons from AA, cutting the electron transfer from CB of $Cs_3Bi_2Br_9$ QDs to BiOBr, which decreases the cathodic photocurrent and $^{\bullet}O_2^-$ generation. Consequently, photogenerated electrons in CB of $Cs_3Bi_2Br_9$ QDs are transferred to the electrode, thereby displaying the inherent anodic photocurrent of $Cs_3Bi_2Br_9$ QDs (Figure 2C).

Overall, a possible mechanism of polarization conversion induced by in situ semiconductor generation and enzyme catalysis is proposed as follows (Scheme 2). First, $Cs_3Bi_2Br_9$ QDs and BiOBr may form a Z-scheme structure, facilitating the electron transfer from CB of BiOBr to VB of $Cs_3Bi_2Br_9$ QDs and resulting in an anodic photocurrent. Second, by furnishing phosphate from AAP, $BiPO_4$ is synthesized on the surface of the $Cs_3Bi_2Br_9$ QDs/BiOBr heterostructure, increasing the E_{CB} of BiOBr more negative than that of $Cs_3Bi_2Br_9$ QDs. Accordingly, a new Z-scheme with a reversed electron-transfer route can be established with the same photoactive materials ($Cs_3Bi_2Br_9$ QDs and BiOBr). Therefore, the first polarization conversion is realized by in situ semiconductor generation, altering anodic photocurrents to cathodic ones. Third, since E_{CB} of BiOBr is more negative than that of $Cs_3Bi_2Br_9$ QDs in the new Z-scheme structure, electrons from donors will preferentially fill photogenerated holes in VB of BiOBr, inhibiting electron transfer from CB of $Cs_3Bi_2Br_9$ QDs to VB of BiOBr. In this case, electrons cannot transfer in the Z-

https://doi.org/10.1021/acs.analchem.1c01457
Anal. Chem. 2021, 93, 8370−8378

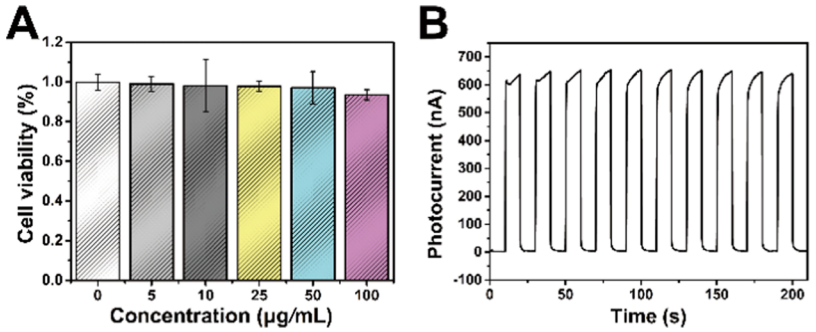

Figure 3. (A) Cell viability of MCF-7 cells treated with different concentrations of the $Cs_3Bi_2Br_9$ QDs/BiOBr heterostructure under irradiation of 490 nm light. (B) Time-based photocurrent response of the $Cs_3Bi_2Br_9$ QDs/BiOBr/$BiPO_4$ heterostructure with AA.

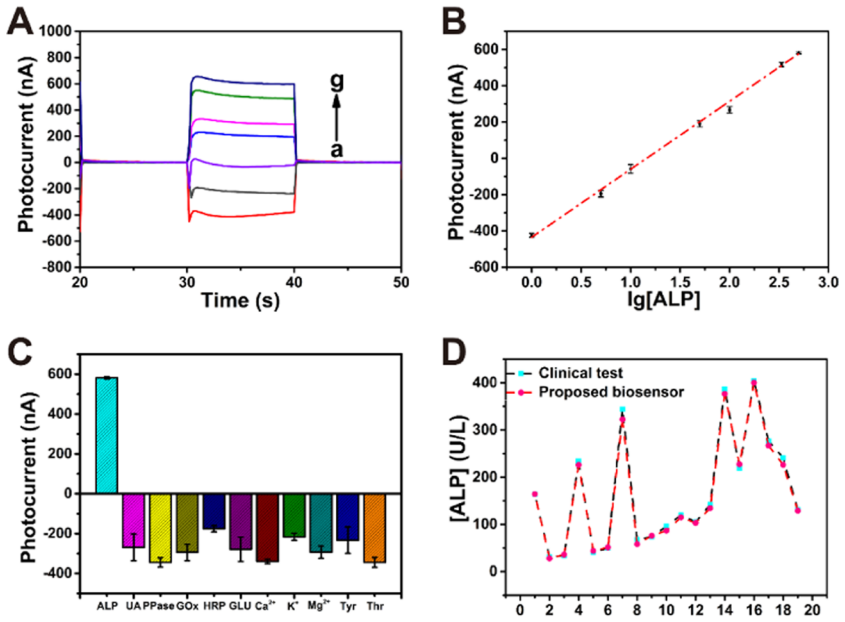

Figure 4. (A) Photocurrent responses of the $Cs_3Bi_2Br_9$ QDs/BiOBr/$BiPO_4$ heterostructure and ALP-treated AAP. From a to g, the concentrations of ALP are 0, 5, 10, 50, 100, 333, and 500 U/L, respectively. (B) Linear dependence of photocurrents on the concentrations of ALP. (C) Photocurrent responses of the $Cs_3Bi_2Br_9$ QDs/BiOBr/$BiPO_4$ heterostructure and AAP treated with ALP and other interfering molecules. (D) Comparison of the measured [ALP] from clinical tests and the proposed PEC biosensor.

scheme manner, and the $Cs_3Bi_2Br_9$ QDs/BiOBr/$BiPO_4$ heterostructure will exhibit inherent PEC behavior of $Cs_3Bi_2Br_9$ QDs. Because AA can be obtained by ALP-induced hydrolysis of AAP, the second polarization conversion is realized by enzyme catalysis, adjusting cathodic photocurrents back to anodic ones. The novel mechanism deepens the understanding of PE principles, which may provide a basis for designing advanced PE systems.

Fabrication of a PEC Biosensor Based on Polarization Conversion of a Perovskite-Based Heterostructure. In comparison with one-wing PEC detection, two-wing detection based on polarization of photoactive materials will enlarge the linear range and improve the sensitivity of relevant methods. In addition, safety and stability of perovskites will be greatly improved by in situ generating other materials as a passivating layer, rendering perovskites suitable for designing bioanalytical methods. Moreover, enzyme catalysis has a high efficiency and specificity. If substrates or products of an enzyme catalysis are electron donors or acceptors, PEC behavior of a photoactive system may be remarkably affected by the enzyme catalysis, enabling selective detection with an ultra-low limit of detection (LOD). Considering the proposed polarization conversion integrates the merits of the two-wing signal switch, semiconductor-protected perovskites, and enzyme catalysis, the $Cs_3Bi_2Br_9$ QDs/BiOBr/$BiPO_4$ heterostructure is further employed to fabricate a PEC ALP biosensor with desirable performance.

Biosafety and stability of the $Cs_3Bi_2Br_9$ QDs/BiOBr/$BiPO_4$ heterostructure were evaluated by the 3-(4,5-dimethylthiazol-2-yl)-2,5-diphenyltetrazolium bromide assays and photocurrent measurements. The growth inhibition of MCF-7 cells treated with the $Cs_3Bi_2Br_9$ QDs/BiOBr heterostructure is shown in Figure 3A, and high cell viability suggests low cytotoxicity of this photoactive material. As shown in Figure 3B, the photocurrents of the $Cs_3Bi_2Br_9$ QDs/BiOBr/$BiPO_4$ heterostructure remain constant after nine on−off cycles of PEC tests, verifying that the $Cs_3Bi_2Br_9$ QDs/BiOBr/$BiPO_4$ heterostructure is adequate to build a stable bioanalytical platform. To pursue the best performance, some conditions for the construction of this PEC biosensor, such as the concentration of AAP, light source, incubation time of enzyme catalysis, and applied potential, were optimized (Figure S9). Under the optimal conditions, the $Cs_3Bi_2Br_9$ QDs/BiOBr/$BiPO_4$ heterostructure exhibits a cathodic photocurrent (−440

https://doi.org/10.1021/acs.analchem.1c01457
Anal. Chem. 2021, 93, 8370−8378

Table 1. Comparison of the Performances of Different ALP Sensors

methods	LOD (U/L)	linear range (U/L)	analysis of human serums (U/L)	ref
fluorescence	5	30−240	233−383	40
fluorescence	1	2.5−40	4−20	41
fluorescence	0.45	1−90	N/A[a]	42
electrochemiluminescence	0.8	5−50	N/A	43
electrochemiluminescence	2	2−25	2.56−15	44
surface-enhanced Raman scattering	1	1−50	N/A	45
electrochemistry	0.94	1−220	42.14	46
electrochemistry	0.5	0.5−20	5−98.5	47
colorimetry	5.4	10−120	N/A	48
photoelectrochemistry	0.33	0.5−40	97	49
photoelectrochemistry	1.5	10−300	N/A	50
photoelectrochemistry	0.15	0.2−15	N/A	51
photoelectrochemistry	0.18	1−500	31−404	this work

[a]"N/A" represents "not applicable."

nA). In the presence of ALP, AAP is hydrolyzed into AA and phosphate. AA can serve as an electron donor and blocks the electron transfer in the $Cs_3Bi_2Br_9$ QDs/BiOBr/$BiPO_4$ heterostructure. With the increase of ALP, more AA is produced, leading to a gradual decrease of cathodic photocurrents and subsequent increase of anodic photocurrents (Figure 4A). It is found that photocurrent of the $Cs_3Bi_2Br_9$ QDs/BiOBr/$BiPO_4$ heterostructure (I) has a linear relation with the concentration of ALP ([ALP]) (Figure 4B). Accordingly, a linear equation I (nA) = 375 lg [ALP] (U/L) − 434 (R = 0.998) is obtained in the range of 1−500 U/L with a LOD of 0.18 U/L. As shown in Table 1, the PEC biosensor reveals a wider linear range and a lower LOD in comparison with other methods for ALP detection, which should be attributed to the superiority of the enzyme catalysis-induced two-wing single switch. In addition, photocurrents of the $Cs_3Bi_2Br_9$ QDs/BiOBr/$BiPO_4$ heterostructure were recorded by treating AAP with other five interfering molecules including pyrophosphatase (PPase), glucose (GLU), glucose oxidase (GOx), horseradish peroxidase (HRP), uric acid (UA), calcium ion (Ca^{2+}), potassium ion (K^+), magnesium ion (Mg^{2+}), tyrosine (Tyr), and threonine (Thr). Since AA cannot be enzymatically produced by other chosen interfering molecules, even another phosphatase, PPase, polarization conversion caused by enzyme catalysis is not observed (Figure 4C). The results confirm that specificity of enzyme catalysis ensures the satisfactory selectivity of this biosensor.

It has been demonstrated that ALP is a biomarker of various cancers,[52] and quantification of ALP is a part of routine physical examination. To verify the applicability of this ALP detection system, 19 human serum samples were collected from a local hospital and tested with our PEC method. According to the obtained results (Figure 4D), concentrations of ALP in these samples are distributed from 31 to 404 U/L, which match well with the data obtained from clinical tests. To our knowledge, [ALP] in serum of healthy people fluctuates in the range of 20−160 U/L. Obviously, concentrations of ALP in some samples are evidently higher than the health threshold. Actually, sample 1 is donated by a patient with obstructive jaundice, while samples 7 and 18 are obtained from patients with liver cancer. In addition, samples 4, 15, 16, and 17 are given by patients with malignant tumors of the pancreas, colon, bone, and stomach, respectively. The above results indicate that our method is accurate and reliable to measure ALP in human serum. Due to the high sensitivity and a low LOD of this method, only 20 μL of serum sample is needed for this biosensor to implement one trial and is much less than the required volume of in use ALP test in hospitals, which further protrudes the value of this method in clinical diagnosis.

CONCLUSIONS

In this work, polarization conversion of perovskite-based photoactive materials is accomplished by in situ semiconductor generation and enzyme catalysis and is used to fabricate a biosensing platform with improved performance. Due to the formation of a Z-scheme structure, the $Cs_3Bi_2Br_9$ QDs/BiOBr heterostructure exhibits a large anodic photocurrent. In the presence of AAP, $BiPO_4$ can be in situ generated on the surface of the $Cs_3Bi_2Br_9$ QDs/BiOBr heterostructure. Since energy bands of BiOBr are increased with the emergence of $BiPO_4$, the electron-transfer route is reversed, leading to the first polarization conversion and signal switch from anodic photocurrents to cathodic ones. However, once AAP is hydrolyzed by ALP, AA is produced to fill photogenerated holes in VB of BiOBr, which impedes electron transfer in the Z-scheme structure. Accordingly, inherent PEC behavior of $Cs_3Bi_2Br_9$ QDs is performed, resulting in the second polarization conversion and signal switch from cathodic photocurrents to anodic ones. Since the signal switch from the cathodic photocurrents to the anodic ones is dependent on the activity of ALP, a PEC ALP biosensor is fabricated based on the perovskite-based heterostructure. Relying on the merits of the two-wing signal switch and enzyme catalysis, ALP can be quantified in a wide range of 1−500 U/L with a low LOD, and ALP in 20 μL of human serum from patients can also be accurately detected. The work achieves polarization conversion of photoactive materials and expands the application of perovskite-based materials, which provides a general strategy for improving the performances of various PE systems.

ASSOCIATED CONTENT

Supporting Information

The Supporting Information is available free of charge at https://pubs.acs.org/doi/10.1021/acs.analchem.1c01457.

Characterization of $Cs_3Bi_2Br_9$ QDs (Figures S1 and S2); band potential measurements of $Cs_3Bi_2Br_9$ QDs, BiOBr, and $BiPO_4$ (Figures S3, S4, and S8); photoelectric responses of $Cs_3Bi_2Br_9$ QDs, BiOBr, $Cs_3Bi_2Br_9$ QDs/BiOBr heterostructure, and AAP (Figure S5); effect of

https://doi.org/10.1021/acs.analchem.1c01457
Anal. Chem. 2021, 93, 8370−8378

AAP on photocurrent responses of the $Cs_3Bi_2Br_9$ QDs/BiOBr heterostructure (Figure S6); ESR measurements of $Cs_3Bi_2Br_9$ QDs/BiOBr/$BiPO_4$ (Figure S7); and optimization of detection conditions (Figure S9) (PDF)

AUTHOR INFORMATION

Corresponding Authors

Zhaoyin Wang − *Jiangsu Collaborative Innovation Center of Biomedical Functional Materials and Jiangsu Key Laboratory of Biofunctional Materials, School of Chemistry and Materials Science, Nanjing Normal University, Nanjing 210023, P. R. China;* orcid.org/0000-0001-7608-8844; Phone: +86-25-85891051; Email: inzo@163.com

Zhihui Dai − *Jiangsu Collaborative Innovation Center of Biomedical Functional Materials and Jiangsu Key Laboratory of Biofunctional Materials, School of Chemistry and Materials Science, Nanjing Normal University, Nanjing 210023, P. R. China;* orcid.org/0000-0001-7049-7217; Email: daizhihuii@njnu.edu.cn

Authors

Hao Yang − *Jiangsu Collaborative Innovation Center of Biomedical Functional Materials and Jiangsu Key Laboratory of Biofunctional Materials, School of Chemistry and Materials Science, Nanjing Normal University, Nanjing 210023, P. R. China*

Min Zhang − *Jiangsu Collaborative Innovation Center of Biomedical Functional Materials and Jiangsu Key Laboratory of Biofunctional Materials, School of Chemistry and Materials Science, Nanjing Normal University, Nanjing 210023, P. R. China*

Lei Wang − *Jiangsu Collaborative Innovation Center of Biomedical Functional Materials and Jiangsu Key Laboratory of Biofunctional Materials, School of Chemistry and Materials Science, Nanjing Normal University, Nanjing 210023, P. R. China*

Renzhong Yu − *Jiangsu Collaborative Innovation Center of Biomedical Functional Materials and Jiangsu Key Laboratory of Biofunctional Materials, School of Chemistry and Materials Science, Nanjing Normal University, Nanjing 210023, P. R. China*

Wenwen Tu − *Jiangsu Collaborative Innovation Center of Biomedical Functional Materials and Jiangsu Key Laboratory of Biofunctional Materials, School of Chemistry and Materials Science, Nanjing Normal University, Nanjing 210023, P. R. China*

Rui Wang − *Jiangsu Collaborative Innovation Center of Biomedical Functional Materials and Jiangsu Key Laboratory of Biofunctional Materials, School of Chemistry and Materials Science, Nanjing Normal University, Nanjing 210023, P. R. China*

Huan Gao − *Jiangsu Collaborative Innovation Center of Biomedical Functional Materials and Jiangsu Key Laboratory of Biofunctional Materials, School of Chemistry and Materials Science, Nanjing Normal University, Nanjing 210023, P. R. China*

Complete contact information is available at: https://pubs.acs.org/10.1021/acs.analchem.1c01457

Notes

The authors declare no competing financial interest.

ACKNOWLEDGMENTS

This work was supported by the National Natural Science Foundation of China (Nos. 21625502 and 21974070) and the Natural Science Foundation of Jiangsu Province of China (Nos. BK20191367 and BK20192008).

REFERENCES

(1) Ma, W.; Fu, P.; Sun, M.; Xu, L.; Kuang, H.; Xu, C. *J. Am. Chem. Soc.* **2017**, *139*, 11752−11759.
(2) Gao, Y.; Nie, W.; Zhu, Q.; Wang, X.; Wang, S.; Fan, F.; Li, C. *Angew. Chem., Int. Ed.* **2020**, *59*, 18218−18223.
(3) Zhan, X. J.; Zheng, J.; Zhao, Y.; Zhu, B. R.; Cheng, R.; Wang, J. Z.; Liu, J.; Tang, J.; Tang, J. Y. *Adv. Mater.* **2019**, *31*, No. 1903329.
(4) Li, H.; Shi, Y. C.; Shang, H.; Wang, W. M.; Lu, J.; Zakharov, A.; Hultman, L.; Uhrberg, R. I. G.; Syväjärvi, M.; Yakimova, R.; Zhang, L. Z.; Sun, J. W. *ACS Nano* **2020**, *14*, 4905−4915.
(5) Yin, Z. Y.; Chen, X. T.; Wang, C.; Guo, Z. J.; Wu, X. L.; Zhao, Z. Y.; Yao, Y. F.; Luo, W. J.; Zou, Z. G. *Chem. Sci.* **2020**, *11*, 6297−6304.
(6) Li, X.; Lu, J. M.; Feng, L. Z.; Zhang, L. Z.; Gong, J. M. *Anal. Chem.* **2020**, *92*, 11476−11483.
(7) Zhao, W. W.; Xu, J. J.; Chen, H. Y. *Chem. Rev.* **2014**, *114*, 7421−7441.
(8) Wang, D. H.; Liu, X.; Fang, S.; Huang, C.; Kang, Y.; Yu, H. B.; Liu, Z. L.; Zhang, H. C.; Long, R.; Xiong, Y. J.; Lin, Y. J.; Yue, Y.; Ge, B. H.; Ng, T. K.; Ooi, B. S.; Mi, Z. T.; He, J. H.; Sun, H. D. *Nano Lett.* **2021**, *21*, 120−129.
(9) Yang, R. Y.; Zou, K.; Zhang, X. H.; Du, C. C.; Chen, J. H. *Chem. Commun.* **2019**, *55*, 8939−8942.
(10) Geng, W. C.; Yang, R. Y. *Chem. Commun.* **2020**, *56*, 2909−2912.
(11) Meng, L. X.; Li, Y. M.; Yang, R. Y.; Zhang, X. H.; Du, C. C.; Chen, J. H. *Chem. Commun.* **2019**, *55*, 2182−2185.
(12) Kim, K. J.; Han, H.; Defferriere, T.; Yoon, D.; Na, S.; Kim, S. J.; Dayaghi, A. M.; Son, J.; Oh, T. S.; Jang, H. M.; Choi, G. M. *J. Am. Chem. Soc.* **2019**, *141*, 7509−7517.
(13) Carrad, D. J.; Bjergfelt, M.; Kanne, T.; Aagesen, M.; Krizek, F.; Fiordaliso, E. M.; Johnson, E.; Nygard, J.; Jespersen, T. S. *Adv. Mater.* **2020**, *32*, No. 1908411.
(14) Yang, T. F.; Zheng, B.; Wang, Y.; Xu, Z.; Pan, T.; Zou, C. J.; Zhang, X. H.; Qi, Z. Y.; Liu, H. J.; Feng, Y. X.; Hu, W.; Miao, D. F.; Sun, L. T.; Duan, X. F.; Pan, A. L. *Nat. Commun.* **2017**, *8*, No. 1906.
(15) Yang, F. L.; Han, P. Y.; Yao, N.; Cheng, G. Z.; Chen, S. L.; Luo, W. *Chem. Sci.* **2020**, *11*, 12118−12123.
(16) Fan, S. D.; Yun, S. J.; Yu, W. J.; Lee, Y. H. *Adv. Sci.* **2020**, *7*, No. 1902751.
(17) Impano, S.; Yang, H.; Jodts, R. J.; Pagnier, A.; Swimley, R.; McDaniel, E. C.; Shepard, E. M.; Broderick, W. E.; Broderick, J. B.; Hoffman, B. M. *J. Am. Chem. Soc.* **2021**, *143*, 335−348.
(18) DeHovitz, J. S.; Loh, Y. Y.; Kautzky, J. A.; Nagao, K.; Meichan, A. J.; Yamauchi, M. S.; MacMillan, D. W. C.; Hyster, T. K. *Science* **2020**, *369*, 1113−1118.
(19) Guo, X. W.; Okamoto, Y.; Schreier, M. R.; Ward, T. R.; Wenger, O. S. *Chem. Sci.* **2018**, *9*, 5052−5056.
(20) Zhao, J. J.; Deng, Y. H.; Wei, H. T.; Zheng, H. P.; Yu, Z. H.; Shao, Y. C.; Shield, J. E.; Huang, J. S. *Sci. Adv.* **2017**, *3*, No. eaao5616.
(21) Lin, Y.-H.; Sakai, N.; Da, P.; Wu, J.; Sansom, H. C.; Ramadan, A. J.; Mahesh, S.; Liu, J.; Oliver, R. D. J.; Lim, J.; Aspitarte, L.; Sharma, K.; Madhu, P. K.; Morales-Vilches, A. B.; Nayak, P. K.; Bai, S.; Gao, F.; Grovenor, C. R. M.; Johnston, M. B.; Labram, J. G.; Durrant, J. R.; Ball, J. M.; Wenger, B.; Stannowski, B.; Snaith, H. J. *Science* **2020**, *369*, 96−102.
(22) Kim, J. Y.; Lee, J. W.; Jung, H. S.; Shin, H.; Park, N. G. *Chem. Rev.* **2020**, *120*, 7867−7918.
(23) Cao, Y.; Zhou, Y.; Lin, Y. H.; Zhu, J. J. *Anal. Chem.* **2021**, *93*, 1818−1825.
(24) Gao, C. M.; Yu, H. H.; Wang, Y. H.; Liu, D. Z.; Wen, T.; Zhang, L. N.; Ge, S. G.; Yu, J. H. *Anal. Chem.* **2020**, *92*, 6822−6826.

(25) Rothmann, M. U.; Kim, J. S.; Borchert, J.; Lohmann, K. B.; O'leary, C. M.; Sheader, A. A.; Clark, L.; Snaith, H. J.; Johnston, M. B.; Nellist, J. P. D.; Herz, L. M. *Science* **2020**, *370*, No. eabb5940.
(26) Lei, Y. S.; Chen, Y. M.; Zhang, R. Q.; Li, Y. H.; Yan, Q. Z.; Lee, S.; Yu, Y. G.; Tsai, H.; Choi, W.; Wang, K. P.; Luo, Y. Q.; Gu, Y.; Zheng, X. R.; Wang, C. F.; Wang, C. H.; Hu, H. J.; Li, Y.; Qi, B. Y.; Lin, M. Y.; Zhang, Z. R.; Dayeh, S. A.; Pharr, M.; Fenning, D. P.; Lo, Y.-H.; Luo, J.; Yang, K. S.; Yoo, J.; Nie, W. Y.; Xu, S. *Nature* **2020**, *583*, 790−795.
(27) Cao, Y.; Zhang, Z. Y.; Li, L. L.; Zhang, J. R.; Zhu, J. J. *Anal. Chem.* **2019**, *91*, 8607−8614.
(28) Huang, Y. P.; Wang, S. Y.; Zhu, Y. M.; Li, F. M.; Jin, J. W.; Dong, J.; Lin, F. Y.; Wang, Y. R.; Chen, X. *Anal. Chem.* **2020**, *92*, 5661−5665.
(29) Li, H.; Zhang, W. *Chem. Rev.* **2020**, *120*, 9835−9950.
(30) Leng, K.; Wang, L.; Shao, Y.; Abdelwahab, I.; Grinblat, G.; Verzhbitskiy, I.; Li, R. L.; Cai, Y. Q.; Chi, X.; Fu, W.; Song, P.; Rusydi, A.; Eda, G.; Maier, S. A.; Loh, K. P. *Nat. Commun.* **2020**, *11*, No. 5483.
(31) Zhao, Q.; Hazarika, A.; Chen, X. H.; Harvey, S. P.; Larson, B. W.; Teeter, G. R.; Liu, J.; Song, T.; Xiao, C. X.; Shaw, L.; Zhang, M. H.; Li, G. R.; Beard, M. C.; Luther, J. M. *Nat. Commun.* **2019**, *10*, No. 2842.
(32) Leng, M. Y.; Yang, Y.; Zeng, K.; Chen, Z. W.; Tan, Z. F.; Li, S. R.; Li, J. H.; Xu, B.; Li, D. B.; Hautzinger, M. P.; Fu, Y. P.; Zhai, T. Y.; Xu, L.; Niu, G. D.; Jin, S.; Tang, J. *Adv. Funct. Mater.* **2018**, *28*, No. 1704446.
(33) Su, D. D.; Han, X. S.; Yan, X.; Jin, R.; Li, H. X.; Kong, D. S.; Gao, H.; Liu, F. M.; Sun, P.; Lu, G. Y. *Anal. Chem.* **2020**, *92*, 12716−12724.
(34) Zheng, X. Z.; Wang, J. H.; Liu, J. J.; Wang, Z. Q.; Chen, S. F.; Fu, X. L. *Appl. Catal., B* **2019**, *243*, 780−789.
(35) Wang, Y.; Li, Y.; Liu, J.; Dong, C.; Xiao, C.; Cheng, L.; Jiang, H.; Jiang, H.; Li, C. *Angew. Chem., Int. Ed.* **2021**, *60*, 7681−7685.
(36) Zhang, Q. X.; Chen, P.; Zhuo, M. H.; Wang, F. L.; Su, Y. H.; Chen, T. S.; Yao, K.; Cai, Z. W.; Lv, W. Y.; Liu, G. G. *Appl. Catal., B* **2018**, *221*, 129−139.
(37) Wang, H.; Zhang, B. H.; Zhao, F. Q.; Zeng, B. Z. *ACS Appl. Mater. Interfaces* **2018**, *10*, 35281−35288.
(38) Wu, Z. H.; Liu, J.; Tian, Q. Y.; Wu, W. *ACS Sustainable Chem. Eng.* **2017**, *5*, 5008−5017.
(39) Kumar, A.; Sharma, S. K.; Sharma, G.; Al-Muhtaseb, A. H.; Naushad, M.; Ghfar, A. A.; Stadler, F. J. *J. Hazard. Mater.* **2019**, *364*, 429−440.
(40) Ma, J.-L.; Yin, B.-C.; Wu, X.; Ye, B.-C. *Anal. Chem.* **2016**, *88*, 9219−9225.
(41) Mei, Y. Q.; Hu, Q.; Zhou, B. J.; Zhang, Y. H.; He, M. H.; Xu, T.; Li, F.; Kong, J. M. *Talanta* **2018**, *176*, 52−58.
(42) Huang, H.; Wang, B.; Chen, M.; Liu, M.; Leng, Y.; Liu, X.; Li, Y.; Liu, Z. *Sens. Actuators, B* **2016**, *235*, 356−361.
(43) Qi, W. J.; Fu, Y. L.; Zhao, M. Y.; He, H. K.; Tian, X.; Hu, L. Z.; Zhang, Y. *Anal. Chim. Acta* **2020**, *1097*, 71−77.
(44) Jiang, H.; Wang, X. *Anal. Chem.* **2012**, *84*, 6986−6993.
(45) Sun, D.; Xu, W. Q.; Liang, C. Y.; Shi, W.; Xu, S. P. *ACS Sens.* **2020**, *5*, 1758−1767.
(46) Hu, Q.; Zhou, B. J.; Dang, P. Y.; Li, L. Z.; Kong, J. M.; Zhang, X. J. *Anal. Chim. Acta* **2017**, *950*, 170−177.
(47) Chen, Z. Q.; Liu, S.; Yu, X. X.; Hao, L. J.; Wang, L.; Liu, S. F. *Analyst* **2019**, *144*, 5971−5979.
(48) Shi, D.; Sun, Y.; Lin, L.; Shi, C.; Wang, G.; Zhang, X. *Analyst* **2016**, *141*, 5549−5554.
(49) Zhang, N.; Ruan, Y. F.; Zhang, L. B.; Zhao, W. W.; Xu, J. J.; Chen, H. Y. *Anal. Chem.* **2018**, *90*, 2341−2347.
(50) Kong, W. S.; Tan, Q. Q.; Guo, H. Y.; Sun, H.; Qin, X.; Qu, F. L. *Microchim. Acta* **2019**, *186*, 73−80.
(51) Tian, J. Y.; Yang, Y. T.; Huang, M. J.; Zhou, C. H.; Lu, J. S. *Talanta* **2019**, *196*, 293−299.
(52) Yang, X. Y.; Bai, Y. Y.; Huangfu, Y. Y.; Guo, W. J.; Yang, Y. J.; Pang, D. W.; Zhang, Z. L. *Anal. Chem.* **2021**, *93*, 1757−1763.

https://doi.org/10.1021/acs.analchem.1c01457
Anal. Chem. 2021, 93, 8370−8378